Selective Crystallization of Four Bis(phthalocyaninato)lanthanoid(III) Polymorphs

*Maegan Dailey, Claire Besson**

Department of Chemistry, The George Washington University, 800 22nd Street NW, Washington, D.C. 20052, United States

ABSTRACT: Bis(phthalocyaninato)lanthanoid(III) ($LnPc_2$) complexes have attracted significant attention for their exceptional optical, electronic and magnetic properties. Crystallization of these compounds usually requires cumbersome methods such as sublimation and electrocrystallization, which is a significant limitation to both structural determinations and the preparation of high purity materials at scale. We report here the selective crystallization of four polymorphs of $LnPc_2$ obtained exclusively by the slow evaporation of saturated solutions. The obtained phase depends on the initial oxidation state of the $LnPc_2$ molecule and the choice of solvent. Single-crystal X-ray diffraction studies were used to determine 14 new structures including Ln = La, Pr, Nd, Sm, Gd, Tb, Dy, Er and Yb, as well as correct previous mis-identifications from the literature. We provide a detailed comparison of molecular structure and crystal packing in all $LnPc_2$ polymorphs. The primary feature in all phases is columnar stacking based on parallel π-π interactions, with a variety of slip angles within those stacks as well as secondary interactions between them. Chemical

redox and acid-base titrations, performed on re-dissolved crystals demonstrate that $LnPc_2^+$ and $LnPc_2^-$ are easily obtained through weak oxidizing and reducing agents, respectively. Additionally, we show that the protonated form of the $NdPc_2^-$ complex has a nearly identical UV-Vis spectra to that of neutral $NdPc_2$, explaining some of the confusion over chemical composition in previously published literature.

INTRODUCTION

Bis(phthalocyaninato)lanthanoid ($LnPc_2$) compounds were first reported by Kirin and Moskalev in the mid-1960s.[1] In these compounds, a trivalent lanthanoid ion is sandwiched between two macrocyclic phthalocyanine (Pc) ligands, with the four isoindole nitrogen atoms of each Pc coordinating to the lanthanoid. The resulting double-decker complexes generally have a square antiprism coordination sphere. Since the 1960s, these species have been intensely studied due to their unique properties, including electrochromism[2], semiconductivity[3], photoconductivity[3], and high chemical and thermal stabilities[4], which arise from the intramolecular π-π interactions of the Pc ligands and the presence of 4*f* orbitals on the metal center.[5] Because of these properties, diphthalocyanine complexes have been integrated in solar cells[6] and field effect transistors[7], and studied as molecular magnets[8] and information storage materials.[9]

Modifications of Kirin and Moskalev's original synthesis resulted in double-decker compounds across the lanthanoid series[10-25] (with the exception of radioactive promethium), as well as for several actinoid[26-31], p-block[32-35], and transition metals.[36] Crystals of varying quality used in structure determinations have been grown through electrochemical methods, solvent-solvent diffusion, and sublimation. Several polymorphs and a dichloromethane solvate phase have been

identified for homoleptic, unsubstituted double-decker compounds (**Table 1**), with the γ-phase, densest of the non-solvated phases, being the most commonly observed.

Table 1. Reported MPc_2 Polymorphs

Phase	α-phase	β-phase	γ-phase	δ-phase	CH_2Cl_2 solvate phase	N/A
Space Group	*P*4/*nnc*	*C*2/*c*	$P2_12_12_1$	*C*2/*c*	*Pnma*	*P*1́
Unit Cell Parameters	*a* = *b* = 19.9 Å *c* = 6.4 Å α = β = γ = 90°[a]	*a* = 19.0 Å *b* = 19.1 Å *c* = 15.5 Å α = γ = 90° β = 116.1° [a]	*a* = 8.8 Å *b* = 10.6 Å *c* = 50.8 Å α= β = γ = 90° [a]	*a* = 28.1 Å *b* = 14.2 Å *c* = 13.2 Å α = γ = 90° β = 115.6° [a]	*a* = 28.1 Å *b* = 22.9 Å *c* = 7.9 Å α = β = γ = 90° [a]	*a* = 13.4 Å *b* = 13.4 Å *c* = 16.3 Å α = 68.7° β = 65.9° γ = 74.7°
Metal Center	Pr,[b,13] Nd,[b,15,17,18] Er,[b,23] Eu,[c,e,31] Am[c,e,31]	Sn,[33] Ce,[b,24] Nd,[b,16] Th,[27,29] Pa,[e,30] U[26,29]	Y,[19,21] In,[32] Sn[33] Nd,[b,e,17], Gd[10], Tb[19,22], Dy[19,22], Lu[11]	Pr,[b,d,12] Nd[c,18]	Y[21], In[e,21], La[b,25] Bi[b,35], Nd[e,14], Tb[21], Lu[10]	Zr[36]

[a] Unit cell parameters of the neodymium complex. [b] Crystals grown by electrochemical methods. [c] Crystallization method unknown. [d] Authors used non standard I2/c space group. [e] Missing coordinates.

Bis(phthalocyaninato)neodymium (III) is unique among the double-deckers in forming the α-[13,17,18], β-[16], γ-[18], δ-[18], and CH_2Cl_2 solvate polymorphs.[14,15] The crystal structures were first reported in the 1980s, typically using crystals grown through electrochemical oxidation of the anionic $LnPc_2^-$ complex, with the exception of the CH_2Cl_2 solvate phase, which was obtained by the re-crystallization of a powder from CH_2Cl_2.[13-18] These methods often resulted in small, low quality crystals or powders that led to mis-identified space groups and/or phase identification

that was only possible by comparison with another complex, with no coordinate determination. Similar difficulties are encountered throughout the lanthanoid series. Though single crystals of functionalized double- and triple-decker (Ln_2Pc_3) complexes have been obtained through solvent-solvent diffusion, there has been limited success with synthesizing $LnPc_2$ in large yields and in growing crystals suitable for X-ray diffraction studies without electrochemical methods.[37-40] This has limited the ability to study the structures of the various polymorphs and their impact on other properties.

Additionally, there has been confusion in the previously published literature about the exact chemical composition of the some of the compounds, in particular for the $NdPc_2$ species.[14,15] Bis(phthalocyaninato)lanthanoid complexes can easily undergo oxidation and reduction reactions to give the charged complexes $LnPc_2^+$ and $LnPc_2^-$, respectively. The neutral and negatively charged species are deep green or purplish blue, while the cation is red, making them perfect candidates for identification by UV-Vis spectroscopy. However, some of the species, e.g. $LnPc_2$ and $HLnPc_2$, can have very similar spectra, and care should be taken in relying solely on UV-Vis spectra for identification.

Here, we report the reproducible and selective crystallization of four of the five known $LnPc_2$ polymorphs, without the use of cumbersome electrochemical methods. An investigation of these polymorphs, conducted by single-crystal X-ray diffraction, allows for a detailed structural comparison between all five polymorphs. Additionally, through chemical titrations, we provide the definitive spectra of charged complexes $NdPc_2^+$ and $NdPc_2^-$ as well as protonated $HNdPc_2$.

EXPERIMENTAL SECTION

Materials and Methods

Lanthanum (III) chloride hydrate (Alfa Aesar), praseodymium (III) chloride hydrate (Strem), neodymium (III) acetate hydrate (Alfa Aesar), samarium (III) chloride hydrate (Alfa Aesar), gadolinium (III) acetate hydrate (BTC), terbium (III) acetate hydrate (Alfa Aesar), dysprosium (III) acetate hydrate (Alfa Aesar), erbium (III) chloride hydrate (Strem), ytterbium (III) acetate hydrate (Alfa Aesar), phthalonitrile (TCI), sodium methoxide (BTC), and hexanol (ACROS) were used as received. Lithium methoxide was prepared by reacting solid lithium metal (Merck) with an excess of dry, degassed methanol (Fisher).

Synthesis of $LnPc_2$ Complexes

All $LnPc_2$ complexes were synthesized according to previously published procedures with some modifications.[10] Phthalonitrile (200 mg, 1.6 mmol), the appropriate lanthanoid (III) salt hydrate (50 mg, cf. list above), and lithium or sodium methoxide (200 mg) were added to a round bottom flask. Hexanol (10 mL) was then added to the flask, and the temperature was increased to 160°C. The mixture was left to reflux for 18.5 hours, after which it was allowed to cool to room temperature. The hexanol was removed under reduced pressure at 65 °C, leaving a blue-green solid. The solid was dissolved in a minimum amount of acetone via sonication, adsorbed onto silica gel, and purified by column chromatography using a CH_2Cl_2/EtOH gradient as eluent. Pure CH_2Cl_2 eluted one dark blue band containing the $LnPc_2^-$ complex. The volume of EtOH was slowly increased to a maximum ratio of 70:30 v:v CH_2Cl_2:EtOH to remove the remaining blue-green and green bands. The green band eluted as one long band that appeared to contain several different shades of green (see Supplementary Information), due to different levels of purity.

UV-Vis analysis of the fractions indicated that the blue-green fractions were a mixture of anionic and neutral phases, while green-yellow fractions were the co-elution of neutral $LnPc_2$ and oligomeric phthalonitrile formed during the reaction. Dark and light green fractions were neutral $LnPc_2$ with no impurities. Pure orange fractions were oligomeric phthalonitrile. Fractions were characterized by UV-Vis spectroscopy after purification was completed. Single crystals for all $LnPc_2$ phases were grown by slow evaporation from a concentrated solution, in air, at room temperature. A solution of neutral $LnPc_2$ in 98:2 v:v $CHCl_3$:EtOH resulted in dark green rectangular plates, determined to be the α-phase, while pure $CHCl_3$ produced dark green blocks shown to be the γ-phase. The δ-phase was produced from a solution of anionic $LnPc_2^-$ in either 98:2 v:v $CHCl_3$:EtOH or pure $CHCl_3$ as dark green rectangular plates. Slow evaporation of a CH_2Cl_2 solution containing neutral $LnPc_2$ or reduced $LnPc_2^-$ resulted in the CH_2Cl_2 solvate phase as green needles of various sizes.

X-Ray Structure Determination

Single crystals were isolated from the bulk samples and mounted on MiTeGen micromounts. Reflection data was collected at 100(2) K with 0.5° ω and/or φ scans on a Bruker SMART diffractometer with an APEX II CCD detector using Mo K_α (λ = 0.71073 Å) radiation. The data was integrated using the SAINT[41] program within the APEX II[42] software suite. An absorption correction was applied using SADABS.[43] All structures were solved with direct methods using SHELXT[44] and refined with SHELXL 2018/3.[45] The WinGX[46] software suite was used to refine the γ-, δ- and CH_2Cl_2 solvate phases of $NdPc_2$ while ShelXle[47] was used to refine all other phases. For every structure, all non-hydrogen atoms were located in difference Fourier maps and refined anisotropically. Aromatic hydrogen atoms, while located in the difference Fourier maps, were placed in position with the HFIX43 command. The hydrogen atoms in the dichloromethane

molecule were placed in position with the HFIX23 command. Platon[48] was used to check all structures for additional symmetry while Mercury[49] was used to visualize structures, generate thermal ellipsoid plots, and create figures. Thermal ellipsoid plots for all phases can be found in the Supporting Information. CCDC Numbers: 2016006-2016009, 2096850-2096867.

Spectroscopic Characterization

Solution UV-Vis spectra were recorded on an Analytik Jena Specord 1500 UV-Vis spectrophotometer. A few drops of concentrated chromatography fractions were placed in a quartz cuvette and diluted with CH_2Cl_2 to a concentration of approx. 2.5×10^{-7} M. For chemical redox titrations, several milligrams of single crystals were isolated from the bulk sample, placed in a quartz cuvette, and dissolved in CH_2Cl_2. Solutions of iodine (I_2, 0.05 M) and triethylamine (NEt_3, 0.05 M) in CH_2Cl_2 were added in microliter increments and UV-Vis spectra were recorded after each addition. This process was repeated, under nitrogen, for acid-base titrations of $NdPc_2$, using concentrated glacial acetic acid, concentrated 1,8-diazabicyclo[5.4.0]undec-7-ene (DBU) and a solution of re-dissolved γ-phase crystals.

Density Functional Theory Calculations

Density function theory (DFT) calculations were performed using Gaussian 16[50] on the high-performance computing cluster at The George Washington University. Initial atomic coordinates were taken from the CH_2Cl_2 solvate phase crystallographic data. Conformation analysis were conducted by freezing the LnN_8 core at the appropriate geometry and optimizing the rest of the molecule at the PBE1PBE[51,52] level of theory using the 6-311g(d,p)[53-55] basis set for H, C, N and Cl. The Stuttgart RSC Segmented basis set with an effective core potential[56-60] for Ln.

Hirshfeld Surfaces

Hirshfeld surfaces and 2D fingerprint plots were generated for all $NdPc_2$ polymorphs using the program Crystal Explorer.[61,62] Surfaces for normalized contact distances are defined by a weight function, which is based on spherically averaged electron atomic densities, and were generated at an isovalue of 0.5 au as implemented in the software. Fingerprint plots map the resulting surface by binning d_i (internal distances; distances from the Hirshfeld surface to the nearest nucleus inside the surface) and d_e (external distances; distances from the Hirshfeld surface to the nearest nucleus outside the surface) pairs in intervals of 0.01 Å, providing information on intermolecular interactions.

RESULTS AND DISCUSSION

The bis(phthalocyaninato)lanthanoid (III) complexes ($LnPc_2$, Ln = La, Pr, Nd, Sm, Gd, Tb, Dy, Er, Yb) are synthesized from phthalonitrile and the appropriate lanthanoid acetate or chloride salt in refluxing hexanol using an approximately 10:1 ratio of phthalonitrile to metal cation. This ratio limits the amount of metal-free phthalocyanine, single- and triple-decker complexes produced in the reaction. Purification by chromatography gives neutral $LnPc_2$ and anionic $LnPc_2^-$, the latter of which slowly re-oxidizes to give the former in solutions exposed to air. Crystallization by slow evaporation gives analytically pure $LnPc_2$, though the conditions of crystallization results in four different polymorphs (**Error! Reference source not found.**): the α-, γ-, δ- and CH_2Cl_2 solvate phases.

Scheme 1. Crystallization conditions for LnPc2 polymorphs.

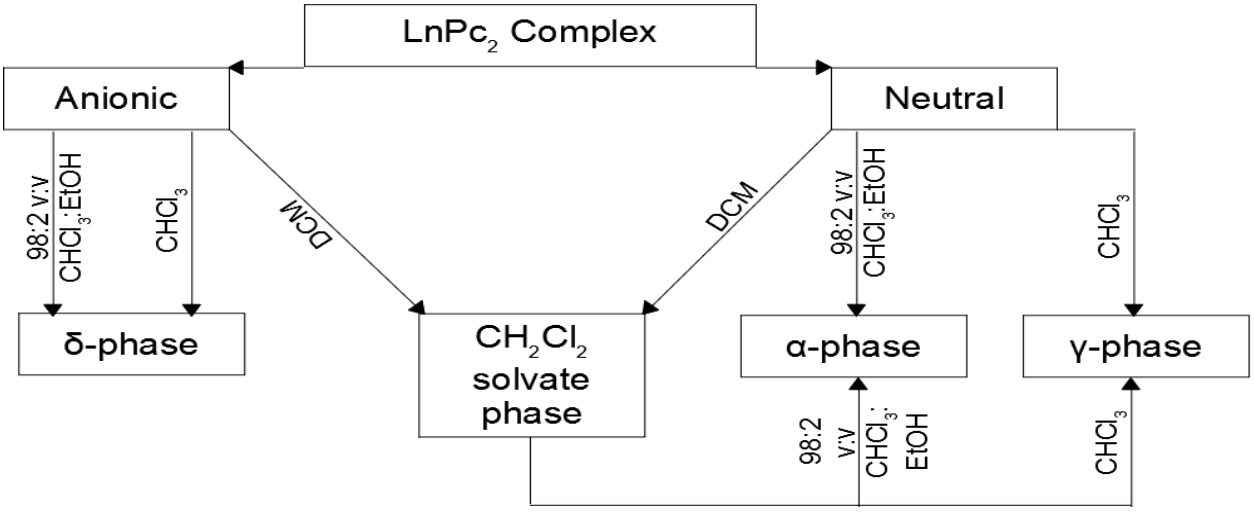

Table 2. $LnPc_2$ polymorphs prepared and characterized by single-crystal X-ray diffraction in this work.

Phase	α-Phase	γ-Phase	δ-Phase	DCM Solvate Phase
Space Group	*P*4/*nnc*	$P2_12_12_1$	*C*2/*c*	*Pnma*
Lanthanoid	La, Nd, Dy	Nd, Sm, Gd, Tb, Dy, Yb	Pr, Nd, Sm, Gd, Tb	La, Pr, Nd, Sm, Gd, Tb, Dy, Er, Yb

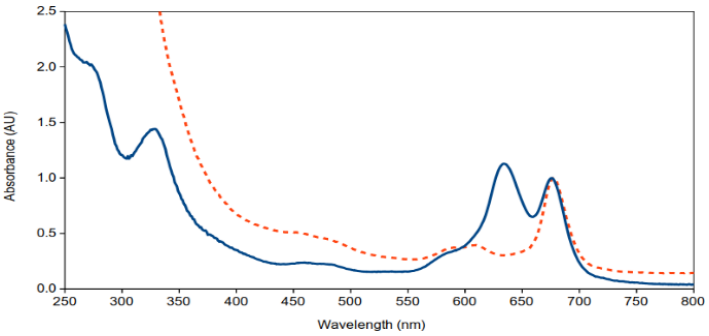

Figure 1. Normalized UV-Vis spectra of the mother liquor of the δ-phase (blue) of $NdPc_2$ and of crystals freshly dissolved in CH_2Cl_2 (red dashes).

The δ-phase is exclusively obtained from mother solutions containing $LnPc_2^-$, which O_2 oxidizes in situ to $LnPc_2$. The anion, however, is not substantially incorporated in the resulting crystal structure, as demonstrated on the example of the neodymium species by the UV-Vis spectrum of dissolved crystals (Figure 1). The spectrum is characteristic of neutral $NdPc_2$ molecules, with three main peaks: a Q band at 678 nm, resulting from a π-π* HOMO-LUMO transition, a broad intervalence band covering the 450-500 nm range, due to the delocalization of a radical electron across both Pc ligands, and a B (or Soret) band around 320 nm corresponding from an additional π-π* transition.[63,64] By contrast, the mother liquor of the δ-phase shows a more intense B band and a split Q band, with one component blue-shifted to 638 nm, characteristic of reduced $LnPc_2^-$.

While the initial oxidation state of the sandwich complex is determinant in the formation of the δ-phase, the choice of solvent is crucial for polymorph selectivity when starting from neutral $LnPc_2$ (Scheme 1): solutions in pure chloroform provide the γ-phase while a 98:2 mixture of chloroform and ethanol yield the α-phase. Dichloromethane, whenever present, is incorporated in the solid to form the $LnPc_2 \cdot CH_2Cl_2$ solvate phase. Interconversion between polymorphs is readily accomplished by dissolving crystals in the appropriate solvent and allowing the saturated solution to slowly evaporate. We determined the structure of 23 different phases (Table 2) by single-crystal X-ray diffraction. The structure of the neodymium phases will be discussed below as representative of the entire series, as only minor structural differences are observed upon change of the metal center.

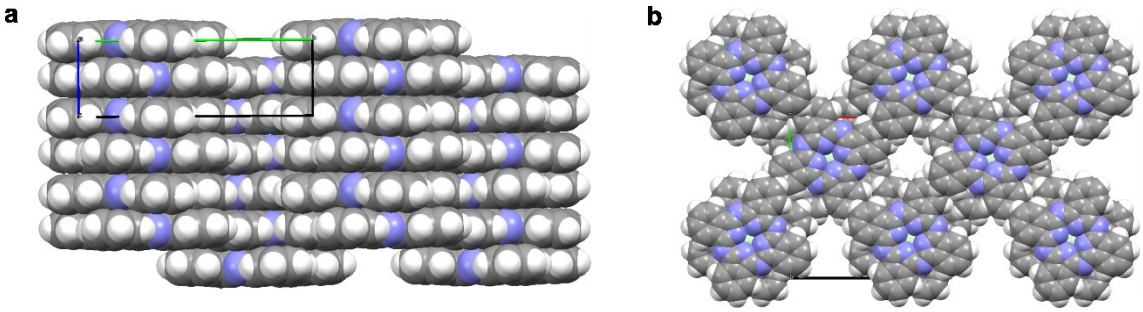

Figure 2. Space-filling model of the structure of the α-$NdPc_2$ phase, viewed along the [100] (a) and the [001] directions (b). Color code: Nd, light green; N, blue; C, grey; H, white.

The α-phase, consistently obtained by slow evaporation of a 98:2 v:v $CHCl_3$:EtOH solution, presents as continuous columns of $NdPc_2$ molecules arranged in a square lattice reminiscent of the typical arrangement observed for $LnPc_2$ mono- and bilayers on metallic surfaces,[19,66-75] but with every second stack displaced vertically by a Pc-Pc distance (Figure 2, Table S2). The asymmetric unit contains 1/8th of the $NdPc_2$ molecule. The remainder of the D_4-symmetry complex is generated by a 4-fold axis and perpendicular 2-fold axes through the Nd^{3+} center. The Nd-N distance is 2.476(5) Å, a value that remains constant across all polymorphs. The Nd^{3+} ion has an approximately square antiprism coordination geometry with a skew angle (Figures 3 and S6) of 40.9° between the two slightly curved Pc rings. Molecules within the columns interact via cofacial π-π stacking[65] (slip angle φ = 90 °, twist angle ψ = 0, Nd-Nd distance 6.4202(16) Å), while stacks are separated by weak H···H contacts at a distance of 2.3077(5) Å. Additionally, a 87:13 disorder is observed between two neodymium positions related by a vertical shift of the $NdPc_2$ column by the length of one Pc-Pc spacing.

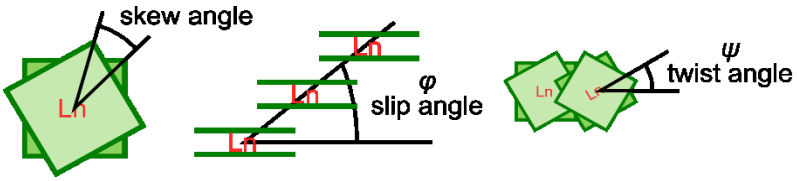

Figure 3. Definition of the skew, slip and twist angles with phthalocyanine rings schematized as squares.

This disorder, combined with the high symmetry space group, have contributed in the past to a number of errors in both space group and structure determination.[13,17,76] In their neodymium structure, Mossoyan-Deneux *et al*. assigned the minor metal contribution as a fractional oxide or chloride anion,[76] a hypothesis which can easily be dismissed based on the UV-visible spectra of the freshly dissolved crystals showing no $NdPc_2^+$ signal. In their study of the praseodymium and neodymium phases Darovsky *et al*. observed a 72:28 disorder between the two metal positions, which they modeled as a 3×3×1 supercell of columns alternatively shifted by *c*/2, accounting for a 75:25 disorder ratio. Darovsky described the additional disorder as due to the presence of small amounts of the triple decker complex Ln_2Pc_3. However, we found no evidence of a super-cell or super-structure in our diffraction data (Figure S7), in agreement with our significantly lower disorder ratio of 87:13. Triple decker Nd_2Pc_3 complexes were not detected in our UV-visible investigations, nor would they be present in samples of the α-phase obtained by recrystallization of another polymorph. Given the weakness of the inter-column interactions (weak H···H contacts, no interlocking molecules), and the resulting low enthalpy cost of the shift of a $LnPc_2$ column across the whole crystal, we hypothesize that the observed disorder is exclusively due to random surface alignment defects propagated throughout the growth of the crystal. An analysis of the Hirshfeld surface and corresponding fingerprint plot (Figure 4) confirms that aside from π-π stacking (5.8%, green color on Figure 4b), the main intermolecular interactions are H···H contacts (61.2%, blue color on Figure 4b). Interestingly, we did not observe any appreciable

disorder in the structures of α-$LaPc_2$ and α-$DyPc_2$, nor was any reported[23] in the structure of α-$ErPc_2$.

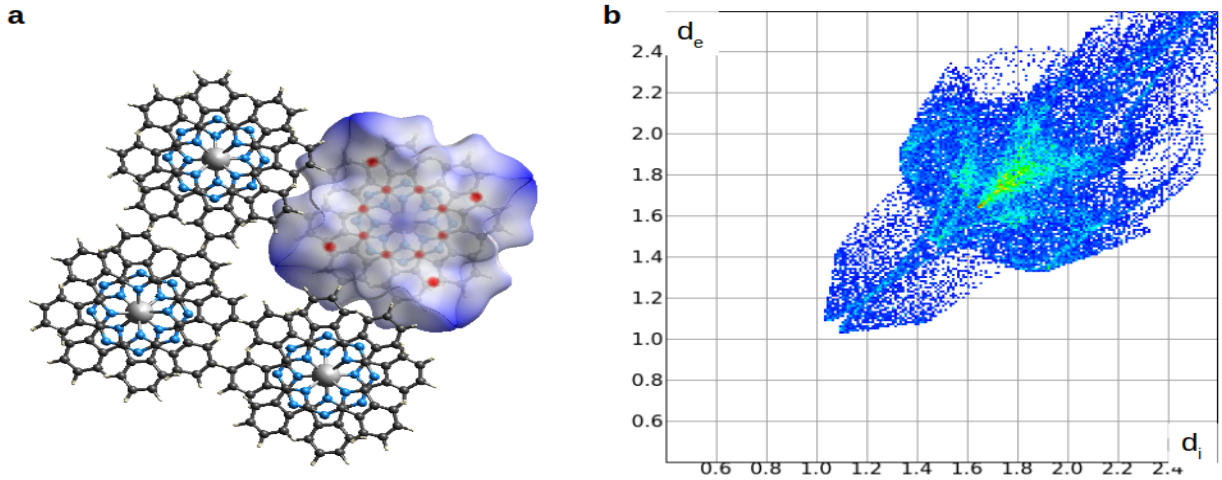

Figure 4: Hirshfeld surface generated for a $NdPc_2$ molecule in the α-phase (a) and the corresponding fingerprint plot (b).

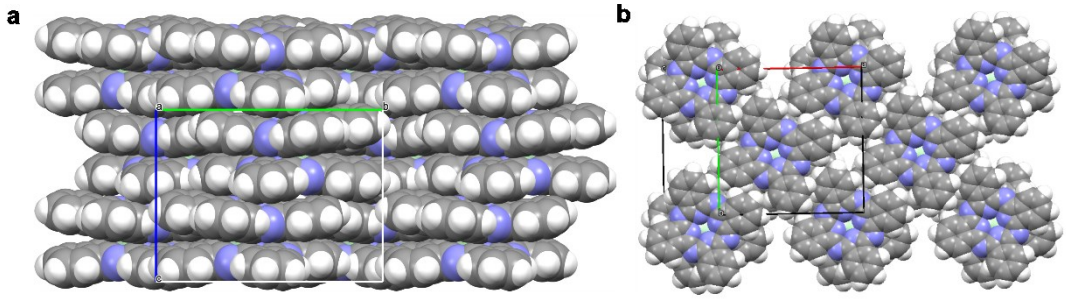

Figure 5. Space-filling model of (a) the structure of the β-$NdPc_2$ phase, viewed along the [100] direction and (b) the monolayer of complexes formed in the (110) plane. Color code: Nd, light green; N, blue; C, grey; H, white. Hydrogen atoms have been added to the published structure to facilitate comparison between the polymorphs.

The β-phase was previously grown by electrochemical methods[16] and could not be reproduced by either slow evaporation or solvent-solvent diffusion in this work. We will give here, for the sake of completion, a brief description of the structure of β-$NdPc_2$ as reported by Darovskikh et al.[16] The C_2-symmetry $NdPc_2$ molecule is generated from the asymmetric unit (one Pc ring and half the Nd center) by a 2-fold axis that runs parallel to the Pc ring and through the Nd^{3+} center. The resulting molecule has a square antiprism geometry with Nd-N distances of 2.46-2.48 Å and a skew angle of 39.0°(±1.2). Compared to the α-phase, the Pc ligands in this phase have a much more pronounced saucer-shape. The double-decker complexes are assembled via by π-π parallel-displaced slipped stacking[65] in stacks progressing in zig-zag along the [100] direction Figure 5a). The slip angle within the stack is $\varphi = 49.5^{o}$, corresponding to a Nd-Nd distance of 8.458 Å. The molecule-to-molecule twist angle of $\psi = -39^{o}$ is opposite to the skew angle, yielding a parallel alignment of the Pc rings facing each other. The stacks are arranged, via H···H contacts at 2.111 and 2.265 Å, in a square lattice almost identical to that of the α phase, but here without any vertical displacement (Figure 5b). The Hirshfeld surface and corresponding fingerprint plot for the β-phase are much like that of the α-phase, showing that the primary intermolecular iteractions are weak H-H contacts and π-π stacking. The plots for this and the remaining phases can be found in the supporting information (Figures S9, S11, S14 and S17).

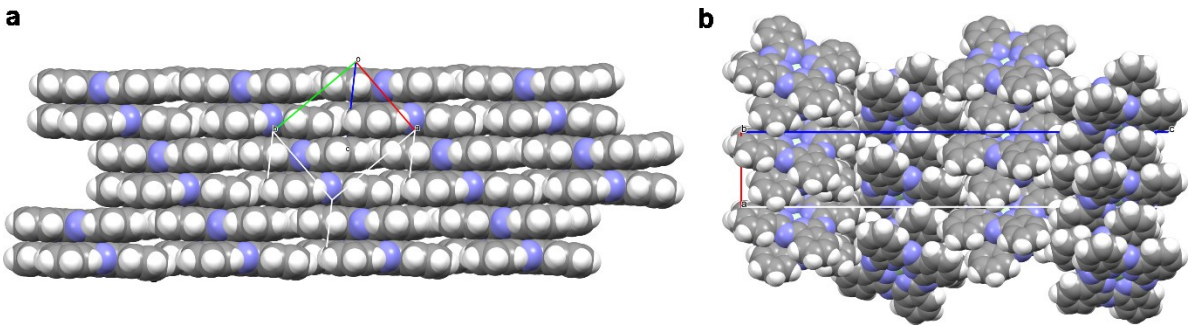

Figure 6. Space-filling model of the structure of the γ-$NdPc_2$ phase, viewed along the $[\bar{1}\bar{1}2]$ (a) and the [010] directions (b). Color code: Nd, light green; N, blue; C, grey; H, white.

The γ-phase of $NdPc_2$ was first identified in 1984 by comparing its powder pattern to that of the previously investigated $SnPc_2$ γ-phase,[76] however, no single-crystal studies have been conducted until this report. The asymmetric unit in this phase is the full $NdPc_2$ molecule, showing barely curved Pc rings and the expected approximately square antiprismatic coordination mode, with Nd-N bond lengths in the range 2.455(3)-2.475(3) Å and a skew angle of 40.8°(±0.3). Parallel-displaced π-π interactions organize the $NdPc_2$ complexes in sheets along the (110) plane, with a bricklayer type stacking (slip angles $\varphi_1 = 47.3^o$, $\varphi_2 = 40.8^o$, twist angles $\psi_1 = \psi_2 = 0$). Nearest Nd-Nd distances within the sheets are 8.852(2) and 10.604(2) Å (Figure 6a). Successive sheets are rotated by 90º along the *c* axis, inducing alternating angles of 81.78(15)º and 85.33(15)º between the Pc-Pc axes of neighboring sheets (**Error! Reference source not found.**b). Contact between the sheets corresponds to edge-on H···H contacts at a distance of 2.30-2.32 Å.

The δ-phase, identified for the first time in 1986, was initially referred to as the β_2 polymorph, as it shares the *C*2/*c* space group of the β-phase.[18] The reported structure lacks H atoms and shows abnormal puckering in some of the benzene rings in the Pc ligands. X-ray diffraction studies

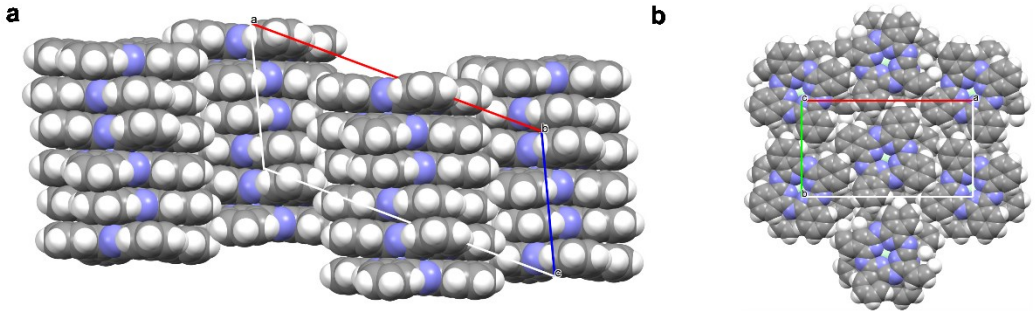

Figure 7. Space-filling model of the structure of the δ-$NdPc_2$ phase, viewed along the [010] (a) and the [001] directions (b). Color code: Nd, light green; N, blue C, grey; H, white.

conducted on crystals grown from solutions of air-oxidized $NdPc_2^-$ allow us to now correct the record. In the δ-phase as in the β-phase, the asymmetric unit of the delta-phase is ½ the molecule, with the full molecule generated by a 2-fold axis through the Nd^{3+} center parallel to the Pc ring. The resulting C_2 symmetry $NdPc_2$ complex displays Nd-N distances in the 2.468(3)-2.473(3) Å range and a skew angle of 42.7°(±0.5), higher than in the α-γ phases but still lower than the 45° value of an ideal square antiprism. The $NdPc_2$ molecules are assembled via slipped stacking π-π interactions[65] in vertical zig-zag columns (slip angle φ = 67°), with the shortest Nd-Nd distance of 7.0782(6) Å (Figure 7a). This particular columnar arrangement is correlated with an atypical curvature of the Pc rings, which take here a sigmoidal shape rather than the more commonly observed saucer shape. As in the β-phase, the Pc rings facing each other are aligned, as the twist angle ψ = -42.7° exactly compensates for the skew angle. Instead of the square lattice observed for the α- and β-phases, the stacks in the δ-phase are arranged in a hexagonal lattice (Figure 7b), similar to what has been observed for self-assembled monolayers of some substituted phthalocyanine complexes.[67] The shortest distances between the interwoven neighboring stacks correspond to C···H and H···H distances of 2.782(4) Å and 2.31901(15) Å, respectively.

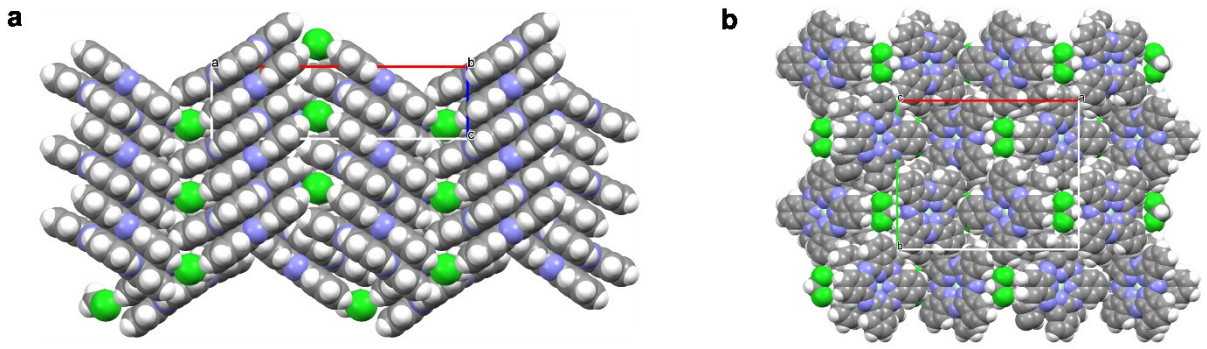

Figure 8. Space-filling model of the structure of the $NdPc_2 \cdot CH_2Cl_2$ phase, viewed along the [010] direction (a) and the [001] directions (b). Color code: Nd, light green; N, blue; Cl, bright green; C, grey; H, white.

The last polymorph is a CH_2Cl_2 solvate phase which has also been previously identified for La, Nd, Tb and Lu. However, the space group was mis-assigned as $P2_12_12_1$ instead of *Pnma* in the case of the neodymium complex.[14] The asymmetric unit in this phase is again ½ the molecule, with the full molecule generated by a mirror plane perpendicular to the Pc rings, imposing a skew angle of exactly 45°. The metal-ligand distances (2.4629(19)-2.477(3) Å) are identical with those of the other phases. Packing in this phase can be described by the formation of slipped columns of $NdPc_2$ complexes via parallel π-π interactions (slip angle φ = 55.3 °, twist angle ψ = 0, Nd-Nd distance 7.8897(4) Å), which are arranged in zig-zag chains (H···H = 2.38428(9) Å) oriented perpendicular to the slip direction to form corrugated sheets (Figure 8). The dichloromethane molecules fill the corrugations. Finally, the planes of the Pc rings in alternate sheets are tilted by 70 ° to give a herringbone-type structure. Note however that contact between the sheets are limited to relatively short N···H distances (2.64371(10) Å), and that no edge-to-face π-π interactions take place in the structure.

We conducted DFT calculations to investigate the stability of the double-decker complexes as a function of the skew angle between the phthalocyanine moieties. The results for the singlet state of $YbPc_2$, which results from an antiferromagnetic coupling between the Yb^{III} center and the radical localized on the phthalocyanine rings, are shown Figure 9. Similar profiles are obtained for the ferro- and antiferromagnetic states of $NdPc_2$, $SmPc_2$ and $GdPc_2$ (Figures S19, S23 and S28). A relatively broad minimum is observed for angles above 40°, in good agreement with the range of skew angles (39.0−45°) observed experimentally.

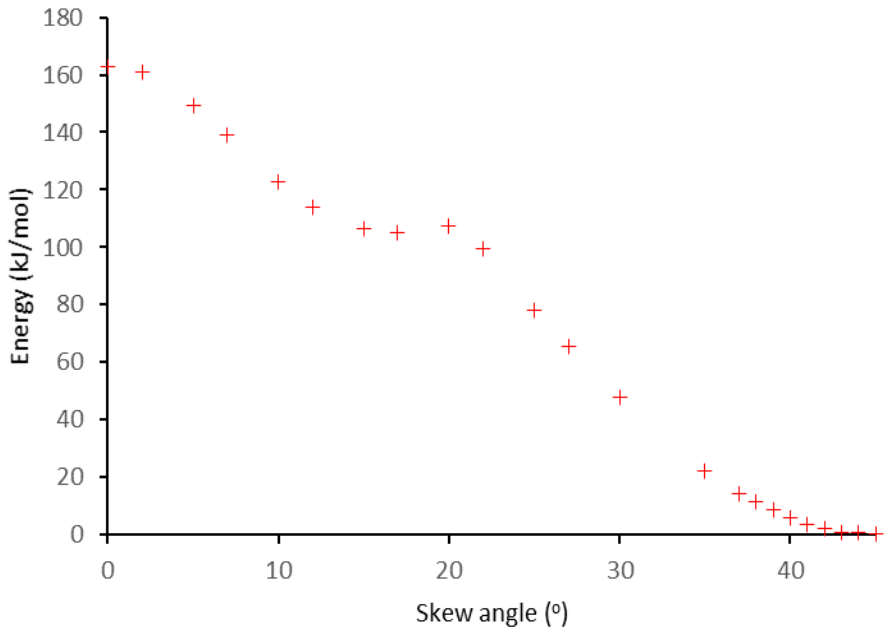

Figure 9. Influence of the skew angle of an $YbPc_2$ molecule on the energy of its singlet state (antiferromagnetic coupling between the Yb^{3+} center and the phthalocyanine radical).

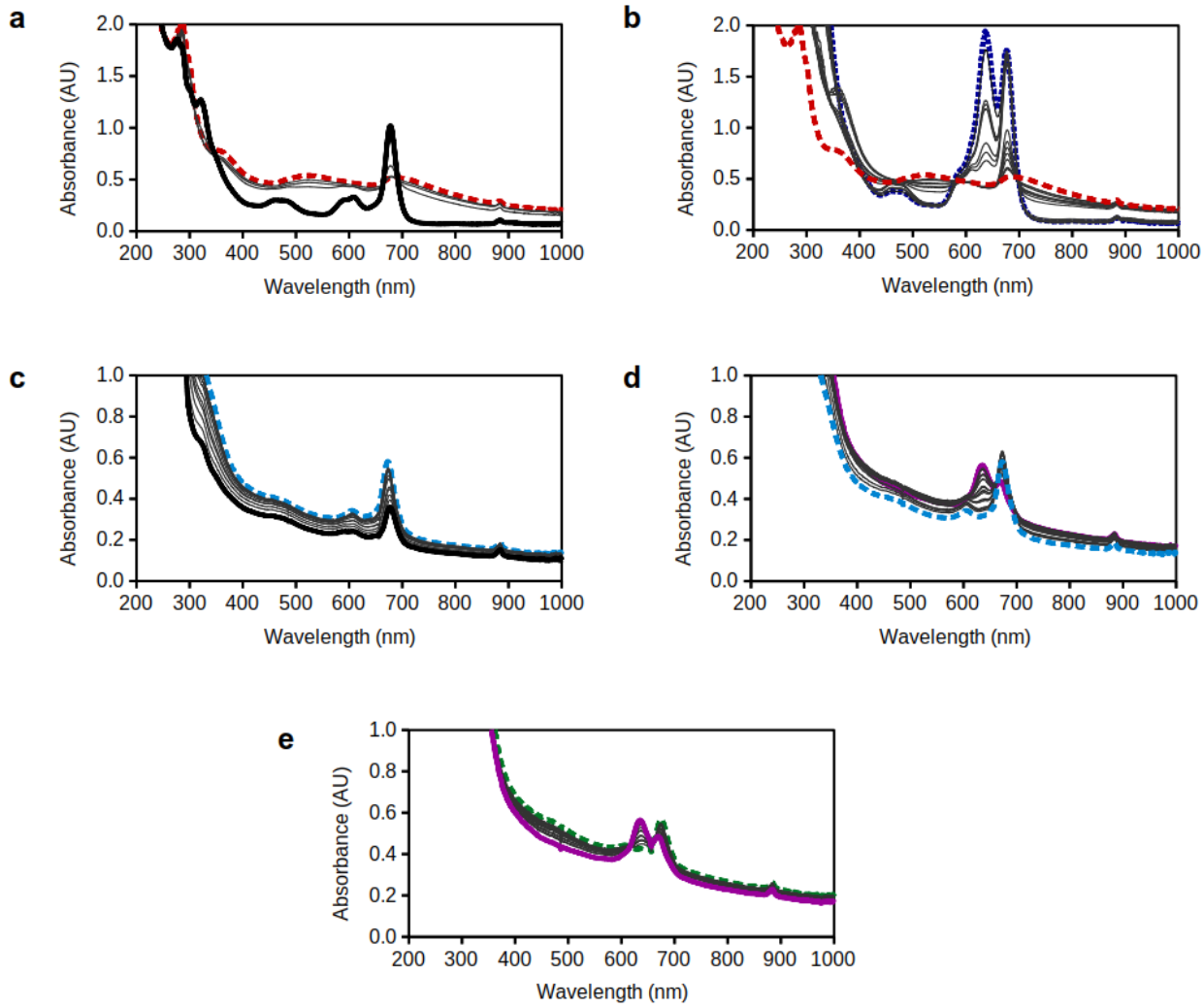

Figure 10. Spectrophotometric titrations of double-decker neodymium complexes. a) Addition of I_2 (0.05 M in CH_2Cl_2, approx. 200 eqv.) to a solution of freshly dissolved α-phase crystals in CH_2Cl_2 oxidizes neutral $NdPc_2$ (approx. 5×10^{-7} M, solid black line) to $NdPc_2^+$ (dashed red line). b) Subsequent addition of NEt_3 (0.05 M in CH_2Cl_2 approx. 3550 eqv.) reduces $NdPc_2^+$ to $NdPc_2^-$ (dotted blue line). c) Addition of acetic acid (approx.3.2×10^5 eqv.) to a solution of freshly dissolved γ-phase crystals in CH_2Cl_2 protonates $NdPc_2$ (solid black line) to $HNdPc_2^+$ (dashed blue line). d) Subsequent addition of DBU (approx. 7.90×10^5 eqv.) deprotonates and reduces $HNdPc_2^+$ to $NdPc_2^-$ (solid purple line). e) Subsequent addition of more acetic acid (approx. 1.60×10^6 eqv.) to the previous solution finally gives $HNdPc_2$ (dashed green line).

Table 3. UV-visible absorption characteristics of $NdPc_2$ derivatives.

Species	$NdPc_2$	$NdPc_2^-$	$NdPc_2^+$	$HNdPc_2^+$	$HNdPc_2$
Q-Band Wavelength (nm)	678	638, 675	687	677	676

In previously published literature, the $NdPc_2{\cdot}CH_2Cl_2$ phase was mistakenly described with the chemical composition $NdPc_2H{\cdot}CH_2Cl_2$, with the additional proton delocalized over the eight chemically equivalent isoindole nitrogen atoms.[14] Despite an X-ray photoelectron spectroscopy study, the authors were unable to prove the existence of the acidic H^+ in the structure. In order to provide definitive references for the easy identification of $NdPc_2$, reduced protonated $NdPc_2H$ and other related species including protonated $HNdPc_2^+$, oxidized $NdPc_2^+$ and reduced $NdPc_2^-$, we recorded the UV-visible spectra of those species, obtained by chemical redox and acid-base titrations of high purity samples of $NdPc_2$ (Table 3, **Error! Reference source not found.**, S12, S15 and S18).[77] Oxidation by I_2, a kinetically fast process, yields $NdPc_2^+$, characterized by a red shift of the Q band, while $NdPc_2^-$ is obtained by slow reduction by NEt_3 and shows a split Q band. Addition of a large excess of concentrated glacial acetic acid to a solution of $NdPc_2$ yields $HNdPc_2^+$, which displays a very slightly red-shifted Q band and an additional peak at 605 nm. Deprotonation and simultaneous reduction of $HNdPc_2^+$ by a large excess of concentrated DBU or NEt_3 yields $NdPc_2^-$, which is protonated by a large excess of concentrated glacial acetic acid to $HNdPc_2$. The resulting $HNdPc_2$ has a very similar spectrum to that of neutral $NdPc_2$, explaining in part the confusion in the previous literature. We therefore recommend that any future speciation done on the basis of UV-Visible spectroscopy include careful titrations of the material.

CONCLUSIONS

Our investigation of $LnPc_2$ crystallization showed that is possible to selectively grow crystals of four polymorphs by solvent slow evaporation, a convenient method affording larger amounts of material and better quality crystals than the previously reported electrochemical techniques. Good single crystals of these polymorphs allowed for a detailed structural analysis through single-crystal X-ray diffraction studies, including 14 new structural determinations and the correction of some mis-identifications in the previously published literature. The packing in all five known polymorphs is dominated by columnar stacking due to parallel π-π interactions, but some significant differences appear between phases in the arrangement of the columns, which is expected to have a significant impact on the conductivity properties of the material. The different polymorphs also exhibit a range of Ln-Ln distances (6.42-8.85 Å for Ln=Nd) and skew angles at the Ln center (39-45°) which will affect the magnetic properties. Additional studies are underway to fully explore the electronic and magnetic properties of these various polymorphs.

ASSOCIATED CONTENT

Crystallographics parameters, bond lengths, thermal ellipsoid plots and checkCIF files for all structures; additional geometric parameters and Hirshfeld plots for the $NdPc_2$ phases, spectrophotometric redox titration of $LnPc_2$ (Ln = Nd: γ, δ and solvate phases, Ln = Sm: solvate phase); skew angle dependence of the energy of $SmPc_2$, $GdPc_2$ and $YbPc_2$ are provided in the Electronic Supplementary Information. Structures deposited under CCDC Numbers 2016006-2016009, 2096850-2096867 and 2108638.

AUTHOR INFORMATION

Corresponding Author

*Claire_Besson@gwu.edu.

Author Contributions

M. D. performed the experiments and calculations, analysed the data, wrote the original draft and edited and reviewed the manuscript. C. B. conceived the idea, supervised the project, analyzed the data and reviewed and edited the manuscript.

ACKNOWLEDGMENT

The authors would like to thank the Cahill group of the George Washington University for the use of their single-crystal X-ray diffractometer. Maegan Dailey would especially like to thank J. August Ridenour of the Cahill group for always freely sharing his expertise. This material is based upon work supported by the National Science Foundation under Grant No. 1800108.

REFERENCES

1. Kirin, I.S.; Moskalev, P.N.; Makashev, Y.A. Formation of Phthalocyanines of Rare-Earth Elements. *Zh Neorg Khim.* **1965**, *10*, 1951-1953.

2. Lenzoff, C.C.; Lever, A.B.P. *Phthalocyanines- Properties and Applications;* New York, 1989-1996

3. McKeown, N.B. *Phthalocyanine Materials- Synthesis, Structure and Function;* Cambridge University Press, New York, 1998.

4. Kadish, K.M.; Smith, K.M.; Guilard, R. *The Porphyrin Handbook Vol. 1-10;* Academic Press, San Diego, 2000.

5. Jiang, J.; Ng, D. A Decade Journey in the Chemistry of Sandwich-Type Tetrapyrrolato-Rare Earth Complexes. *Acc. Chem. Res.,* **2009**, *42*, 79-88.

6. Videlot, C.; Fichou, D.; Garnier, F. Photovoltaic Solar Cells Based on Rare-Earth Bisphthalocyanine Complexes. *Mol. Cryst. Liq. Cryst.*, **1998**, *322*, 319-328.

7. Chen Y.; Su, W.; Bai, M.; Jiang, J.; Li, X.; Liu, Y.; Wang, L.; Wang, S. High Performance Organic Field-Effect Transistors Based on Amphiphillic Tris(phthalocyaninato) Rare Earth Triple-Decker Complexes. *J. Am. Chem. Soc.*, **2005**, *127*, 15700-15701.

8. Ishikawa, N.; Sugita, M.; Wernsdorfer, W. Quantum Tunneling of Magnetization in Lanthanide Single-Molecule Magnets: Bis(phthalocyaninato)terbium and Bis(phthalocyaninato)dysprosium Anions. *Angew. Chem., Int. Ed.*, **2005**, *44*, 2931-2935.

9. Liu, Z.; Yasseri, A.A.; Lindsey, J.S.; Bocian, D.F. Molecular Memories that Survive Silicon Device Processing and Real-World Operation. *Science,* **2003**, *302*, 1543-1545.

10. De Cian, A.; Moussavi, M.; Fischer, J.; Weiss, R. Synthesis, Structure, and Spectroscopic and Magnetic Properties of Lutetium (III) Phthalocyanine Derivatives: $LuPc_2 \cdot CH_2Cl_2$ and $[LuPc(OAc)(H_2O)_2]H_2O \cdot 2CH_3OH$. *Inorg. Chem.*, **1985**, *24*, 3162-3167.

11. Darovskikh, A.N.; Frank-Kamenetskaya, O.V.; Fundamenskii, V.S.; Golubev, A.M. The Crystal and Molecular Structure of Lutetium Diphthalocyanine (γ-Phase). *Kristallografiya,* **1986**, *31*, 279-283.

12. Darovsky, A.; Wu, L. Y.; Lee, P.; Sheu, H. S. Structure of Bis(phthalocyaninato)praseodymium (β1 Phase). *Acta. Cryst.,* **1991**, *C47*, 1836-1838.

13. Darovsky, A.; Keserashvili, V.; Harlow, R.; Mutikainen, I. Structure of Oxidized Forms of Neodymium and Praseodymium (Bis)Phthalocyanines. *Acta Cryst.*, **1994**, *B50*, 582-588.

14. Kasuga, K.; Tsutsui, M.; Petterson, R.C.; Tatsumi, K.; Van Opdenbosch, N.; Pepe, G.; Meyer, E.F. Structure of Bis(phthalocyaninato)neodymium (III). *J. Am. Chem. Soc.*, **1980**, *102*, 4836-4838.

15. Sullivan, B.W.; Dominey, R.; Helms, J.; Schwartz, M.; ter Haar, L.; Hatfield, W. Preparation and Properties of Single Crystals of Hydrogen Bis(Phthalocyaninato) Neodymium(III). *Mol. Cryst. Liq. Cryst.*, **1985**, *120*, 433-436.

16. Darovskikh, A.N.; Tsytsenko, A.K.; Frank-Kamenetskaya, O.V.; Fundamenskii, V.S.; Moskalev, P.N. Polymorphism of Diphthalocyanine-Neodymium. Molecular and Crystal Structure of β Phase. *Sov. Phys. Crystallogr.*, **1984**, *24*, 273-276.

17. Darovskikh, A. Molecular and Crystal Structure of Tetragonal α-Phase of Neodymium Diphthalocyanine. *Krystallografya*, **1986**, *31*, 901-905

18. Jullien, J.; Mossoyan-Déneux, M.; Pierrot, M.; Sorbier, J.; Fournel, A.; Benlian, D. On Two Conductive Species Derived from Bis(phthalocyaninato) Neodymium. *C. R. Acad. Sc. Paris.*, **1986**, *303*, 669-672.

19. Katoh, K.; Komeda, T.; Yamashita, M. Surface Morphologies, Electronic Structures, and Kondo Effect of Lanthanide(III)-Phthalocyanine Molecules on Au(111) by using STM, STS, and FET Properties for Next Generation Devices. *Dalton Trans*., **2010**, *39*, 4708-4723.

20. Komijani, D.; Ghirri, A.; Bonizzoni, C.; Klyatskaya, S.; Moreno-Pineda, E.; Ruben, M.; Soncini, A.; Affronte, M.; Hill, S. Radical-Lanthanide Ferromagnetic Interation in a TbIII Bis-Phthalocyaninato Complex. *Phys. Rev. Mater.,* **2018**, *2*, 024405.

21. Ostendorp, G.; Homborg, H. Synthesis and Properties of the Diphthalocyaninates of Yttrium and Indium. *Z. Anorg. Allg. Chem.*, **1996**, *622*, 1358-1364.

22. Katoh, K.; Yoshida, Y.; Yamashita, M.; Miyasaka, H.; Breedlove, B.K.; Kajiwara, T.; Takaishi, S.; Ishikawa, N.; Isshiki, H.; Zhang, Y.; Komeda, T.; Yamagishi, M.; Takeya, J. Direct Observation of Lanthanide(III)-Phthalocyanine Molecules on Au(111) by Using Scanning Tunneling Microscopy and Scanning Tunneling Spectroscopy and Thin-Film Field-Effect Transistor Properties of Tb(III)- and Dy(III)- Phthalocyanine Molecules. *J. Am. Chem. Soc.*, **2009**, *131*, 9967-9976.

23. Ostendorp, G.; Werner, J.; Homborg, H. Bis(phthalocyaninato)erbium (α_1 Phase). *Acta. Cryst.*, **1995**, *C51*, 1125-1128.

24. Haghighi, M.; Teske, C.; Homborg, H. Preparation, Properties and Crystal Structure of Bis(phthalocyaninato)cerium(IV). *Z. Anorg. Allg. Chem.*, **1992**, *608*, 73-80.

25. Ostendorp, G.; Homborg, H. Synthesis, Properties and Crystal Structure of Di(phthalocyaninato)lanthanum(III), a Partially Oxidized Semiconductor. *Z. Naturforssch. B,* **1995**, *50*, 1200-1206.

26. Gieren, A.; Hoppe, W. X-Ray Crystal Structure Analysis of Bisphthalocyaninatouranium (IV). *J. Chem. Soc. D*, **1971**, 413-415.

27. Darovskikh, A.N.; Frank-Kamenetskaya, O.V.; Fundamenskii, V.S.; Golynskaya, O.A. Refinement of the Molecular and Crystal Structure of Thorium Diphthalocyanine: Crystal Chemical Characteristics of a Monoclinic Modification of Diphthalocyanines of Actinides and Rare-Earth Elements. *Kristallografiya,* **1985**, *30*, 1085-1089.

28. Kobayashi, T. Crystal and Molecular Structures of Bisphthalocyaninatothorium (IV). *Bull. Inst. Chem. Res., Kyoto Univ.*, **1978**, *56*, 204-212.

29. Kirin, I.S.; Kolyadin, A.B.; Lychev, A.A. The X-Ray Diffraction Study of Thorium and Uranium Diphthalocyanine Complexes. *Russ. J. Struct. Chem.*, **1974**, *15*, 486-490.

30. Lux, F.; Beck, O.F.; Krauss, H.; Brown, D.; Tso, T.C. Spectroscopically Pure Bis(phthalocyaninato)protactinium(IV). *Z. Naturforsch., B*, **1980**, *35B*, 564-567.

31. Moskalev, P. N.; Shapkin, G.N.; Darovskikh, A.N. Synthesis and Properties of Electrochemically Oxidized Diphthalocyanines of Rare Earth Elements and Americium. *Russ. J. Inorg. Chem.*, **1979**, *24*, 340-346.

32. Jancak, J.; Kubiak, R; Jezierski, A. Synthesis, Crystal Structure, and Magnetic Properties of Indium(III) Diphthalocyanine. *Inorg. Chem.*, **1995**, *34*, 3505-3508.

33. Bennet, W.E.; Broberg, D.E.; Baenziger, N.C. Crystal Structure of Stannic Phthalocyanine, an Eight-Coordinated Tin Complex. *Inorg. Chem.,* **1973**, *12*, 930-936.

34. Janczak, J.; Kubiak, R. Crystal and Molecular Structure of Tin Bisphthalocyanine at 300 K (Monoclinic Form). *J. Alloy Compd.,* **1994**, *204*, 5-11.

35. Ostendorp, G.; Homborg, H. Synthesis and Properties of Diphthalocyaninates of Bismuth, $[Bi(Pc)_2]^k$ (k = 1-, 0, 1+); Crystal Structure of Mixed-Valent $[Bi(Pc)_2]\cdot CH_2Cl_2$. *Z. Anorg. Allg. Chem.*, **1996,** *622,* 873-880.

36. Silver, J.; Lukes, P.; Howe, S.D.; Howlin, B. Synthesis, Structure, and Spectroscopic and Electrochromic Properties of Bis(phthalocyaninato)zirconium(IV). *J. Mater. Chem.*, **1991**, *1*, 29-35.

37. Bian, Y.; Wang, D.; Wang, R.; Weng, L.; Dou, J.; Zhao, D.; Ng, D.; Jiang, J. Structural Studies of the Whole Series of Lanthanide Double-Decker Compounds with Mixed 2,3-Napthalocyaninato and Octaethylporphyrinato Ligands. *New. J. Chem.*, **2003**, *27*, 844-849.

38. Anyhan, M. M.; Singh, A.; Jeanneau, E.; Ahsen, V.; Zyss, J.; Ledoux-Rak, I.; Gürek, A.; Hirel, C.; Bretonnière, Y.; Andraud, C. ABAB Homoleptic Bis(phthalocyaninato)lanthanide(III) Complexes: Original Octupolar Design Leading to Giant Quadratic Hyperpolarizability. *Inorg. Chem.*, **2014**, *53*, 4359-4370.

39. Jiang, J.; Bian, Y.; Furuya, F.; Liu, W.; Choi, M.; Kobayashi, N.; Li, H.; Yang, Q.; Mak, T.; Ng, D. Synthesis, Structure, Spectroscopic Properties, and Electrochemistry of Rare Earth Sandwich Compounds with Mixed 2,3-Naphthalocyaninato and Octaethylporphyrinato Ligands. *Chem. Eur. J.*, **2001**, *7*, 5059-5069.

40. Fahrendorf, S.; Matthes, F.; Bürgler, D. E.; Schneider, C. M.; Atodiresei, N.; Caciuc, V.; Blügel, S.; Besson, C.; Kögerler, P. Structural Integrity of Single Bis(Phthalocyaninato)-Neodymium(III) Molecules on Metal Surfaces with Different Reactivity. *Spin*, **2014**, *4*, 11440007-11440018.

41. *SAINT*; Bruker AXS. Inc.: Madison Wisconsin, USA, 2007.

42. *APEX II*; Bruker AXS Inc.: Madison, WI, 2008.

43. Krause, L.; Herbst-Irmer, R.; Sheldrick, G.M.; Stalke, D. Comparison of Silver and Molybdenum Microfocus X-Ray Sources for Single-Crystal Structure Determination. *J. Appl. Crystallogr.*, **2015**, *48*, 3-10.

44. Sheldrick, G. M. SHELXT - Integrated space-group and crystal-structure determination. *Acta Cryst. A*, **2015**, *71*, 3-8.

45. Sheldrick, G. M. Crystal Structure Refinement with SHELXL. *Acta Crystallogr., Sect. C: Struct. Chem.*, **2015**, *71*, 3-8.

46. Farrugia, L. J. WinGX Suite for Small-Molecule Single-Crystal Crystallography. *J. Appl. Crystallogr.,* **2012**, *45*, 849-854.

47. Hübschle, C.B.; Sheldrick, G.M.; Dittrich, B. ShelXle: a QT Graphical User Interface for SHELXL. *J. Appl. Cryst.*, **44**, *2011*, 1281-1284.

48. Spek, A.L. Single-crystal Structure Validation with the Program PLATON. *J. Appl. Crystallogr.,* **2003**, *36*, 7-13.

49. Macrae, C. F.; Edgington, P. R.; McCabe, P.; Pidcock, E.; Shields, G. P.; Taylor, R.; Towler, M.; van de Streek, J. Mercury: Visualization and Analysis of Crystal Structures. *J. Appl. Crystallogr.*, **2006**, *39*, 453-457.

50. Frisch, M.J.; Trucks, G.W.; Schlegel, H.B.; Scuseria, G.E.; Robb, M.A.; Cheeseman, J.R.; Scalmani, G.; Barone, V.; Petersson, G.A.; Nakatsuji, H.; Li, X.; Caricato, M.; Marenich, A.V.;

Bloino, J.; Janesko, B.G.; Gomperts, R.; Mennucci, B.; Hratchian, H.P.; Ortiz, J.V.; Izmaylov, A.F.; Sonnenberg, J.L.; Williams-Young, D.; Ding, F.; Lipparini, F.; Egidi, F.; Goings, J.; Peng, B.; Petrone, A.; Henderson, T.; Ranasinghe, D.; Zakrzewski, V.G.; Gao, J.; Rega, N.; Zheng, G.; Liang, W.; Hada, M.; Ehara, M.; Toyota, K.; Fukuda, R.; Hasegawa, J.; Ishida, M.; Nakajima, T.; Honda, Y.; Kitao, O.; Nakai, H.; Vreven, T.; Throssell, K.; Montgomery, J.A.; Peralta, J.E.; Ogliaro, F.; Bearpark, M.J.; Heyd, J.J.; Brothers, E.N.; Kudin, K.N.; Staroverov, V.N.; Keith, T.A.; Kobayashi, R.; Normand, J.; Raghavachari, K.; Rendell, A.P.; Burant, J.C.; Iyengar, S.S.; Tomasi, J.; Cossi, M.; Millam, J.M.; Klene, M.; Adamo, C.; Cammi, R.; Ochterski, J.W.; Martin, R.L.; Morokuma, K.; Farkas, O.; Foresman, J.B.; Fox, D.J. Gaussian 16 (Revision C.01), Gaussian, Inc., Wallingford, CT, 2016.

51. Perdew, J.P.; Burke, K.; Ernzerhof, M. Generalized Gradient Approximation Made Simple. *Phys. Rev. Lett.*, **1997**, *77*, 3865-3868.

52. Adamo, C.; Barone, V. Toward Reliable Density Functional Methods without Adjustable Parameters: The PBE0 Model. *J. Chem. Phys.,* **1999**, *110*, 6158-6170.

53. McLean, A.D.; Chandler, G.S. Contracted Gaussian Basis Sets for Molecular Calculations. I. Second Row Atoms, Z = 11-18. *J. Chem. Phys.*, **1980**, *72*, 5639-5648.

54. Krishnan, R.; Binkley, J.S.; Seeger, R.; Pople, J.A. Self-Consistent Molecular Orbital Methods. XX. A Basis Set for Correlated Wave Functions. *J. Chem. Phys.,* **1980**, *72*, 650-654.

55. Wachters, A.J.H. Gaussian Basis Set for Molecular Wavefunctions Containing Third-Row Atoms. *J. Chem. Phys.,* **1969**, *52*, 1033-1036.

56. Pritchard, B.P.; Altarawy, D.; Didier, B.; Gibson, T.; Windus, T. A New Basis Set Exchange: An Open, Up-to-date Resource for the Molecular Sciences Community. *J. Chem. Inf. Model.,* **2019**, *59*, 4814-4820.

57. Feller, D. The Role of Databases in Support of Computational Chemistry Calculations. *J. Comput. Chem.,* **1996**, *17*, 1571-1586.

58. Schuchardt, K.L.; Didier, B.T.; Elsethagen, T.; Sun, L.; Gurumoorthi, V.; Chase, J.; Li, J.; Windus, T.L. Basis Set Exchange: A Community Database for Computational Sciences. *J. Chem. Inf. Model.,* **2007**, *47*, 1045-1052.

59. Cao, X.; Dolg, M. Segmented Contraction Scheme for Small-Core Lanthanide Pseudopotential Basis Sets. *J. Mol. Struc-Theochem.,* **2002**, *47*, 1045-1052.

60. Dolg, M.; Stoll, H.; Preuss, H. Energy-Adjusted Ab Initio Pseudopotentials for the Rare Earth Elements. *J. Chem. Phys.,* **1989**, *90*, 1730-1734.

61. Spackman, P.R.; Turner, M.J.; McKinnon, J.J.; Wolff, S.K.; Grimwood, D.J.; Jayatilaka, D.; Spackman, M.A. CrystalExplorer: A Program for Hirshfeld Surface Analysis, Visualization and Quantitative Analysis of Molecular Crystals. *J. Appl. Cryst.*, **2021**, *54*, 1006-1011.

62. Spackman, M.A.; Jayatilaka, D. Hirshfeld Surface Analysis. *CrystEngComm*, **2009**, *11*, 19-32.

63.McKeown, N.B. Phthalocyanines and Related Compounds. *Sci. Synth.*, **2004**, *17*, 1237.

64. Ostendorp, G.; Homborg, H. Synthesis and Spectroscopical Properties of the Mixed-Valent Di(phthalocyaninato)lanthanides(III). *Z. Anorg. Allg. Chem.*, **622,** *1996*, 1222-1230.

65. Yao, Z.; Wang, J.; Pei, J. Control of π-π Stacking via Crystal Engineering in Organic Conjugated Small Molecule Crystals. *Cryst. Growth Des.,* **18***, 2018*, 7-15.

66. Komeda, T.; Isshiki, H.; Liu, J.; Katoh, K.; Yamashita, M. Variation of Kondo-Temperature Induced by Molecule-Substrate Decoupling in Film Formation of Bis(phthalocyaninato)terbium(III) Molecules on Au (III). *ACS Nano*, **8**, *2014*, 4866-4875.

67. Ara, F.; Qi, Z.; Hou, J.; Komeda, T.; Katoh, K.; Yamashita, M. A Scanning Tunneling Microscopy Study of the Electronic and Spin States of Bis(phthalocyaninato)terbium(III) ($TbPc_2$) Molecules on Ag(III). *Dalton Trans.,* **45**, *2016*, 16644-16652.

68. Serrano, G.; Wiespointner-Baumgarthuber, S.; Tebi, S.; Klyatskaya, S.; Ruben, M.; Koch, R.; Müllegger, S. Bilayer of Terbium Double-Decker Single-Molecule Magnets. *J. Phys. Chem. C.,* **2016,** *120*, 13581-13586.

69. Gottfried, J. Surface Chemistry of Porphyrins and Phthalocyanines. *Surf. Sci. Rep.,* **70***, 2015,* 259-379.

70. Komeda, T.; Isshiki, H.; Liu, J.; Zhang, Y.; Lorente, N.; Katoh, K.; Breedlove, B.; Yamashita, M. Observation and Electric Current Control of a Local Spin in a Single-Molecule Magnet. *Nature Comm.*, **217**, *2011*, 1-7.

71. Gopakumar, T.G.; Brumme, T.; Kröger, J.; Toher, C.; Cuniberti, G.; Berndt, R. Coverage-Driven Electronic Decoupling of Fe-Phthalocyanine from a Ag(111) Substrate. *J. Phys. Chem. C.,* **115**, *2011*, 12173-12179.

72. Zhang, Y.; Isshiki, H.; Katoh, K.; Yoshia, Y.; Yamashita, M.; Miyasaka, H.; Breedlove, B.; Kajiwara, T.; Takaishi, S.; Komeda, T. Low-Temperature Scanning Tunneling Microscopy

Investigation of Bis(phthalocyaninato)yttrium Growth on Au(111): From Individual Molecules to Two-Dimensional Domains. *J. Phys. Chem. C.,* **113**, *2009*, 9826-9830.

73. Fu, Y.; Schwöbel, J.; Hla, S.; Dilullo, A.; Hoffmann, G.; Klyatskaya, S.; Ruben, M.; Wiesendanger, R. Reversible Chiral Switching of Bis(phthalocyaninato) Terbium(III) on a Metal Surface. *Nano Lett.,* **12**, *2012*, 3931-3935.

74. Deng, Z.; Rauschenbach, S.; Stepanow, S.; Klyatskaya, S.; Ruben, M.; Kern, K. Self-Assembly of Bis(phthalocyaninato)terbium on Metal Surfaces. *Phys. Scr.,* **90**, *2015*, 1-9.

75. Inose, T.; Tanaka, D.; Tanaka, H.; Ivasenk, O.; Nagata, T.; Ohta, Y.; De Feyter, S.; Ishikawa, N.; Ogawa, T. Switching of Single-Molecule Magnetic Properties of Tb^{III}-Porphyrin Double-Decker Complexes and Observation of Their Supramolecular Structures on a Carbon Surface. *Chem. Eur. J.,* **20**, *2014*, 11362-11369.

76. Mossoyan-Deneux, M.; Benlian, D.; Baldy, A.; Pierrot, M. Crystal Structures of Tetragonal $NdPc_2O$ and $NdPc_2Cl_xO_{1-x}$ Obtained from $NdPc_2H$ by Anodic Crystal Growth. *Mol. Cryst. Liq. Cryst. Inc. Nonlin. Opt.,* **1988**, *156*, 247-256.

77. The spectra of some of those species reported previously occasionally suffer from miss-assignment of protonation or redox states and/or aggregation issues leading to broadened spectra. Molar absorption coefficients, when present, vary greatly from reference to reference, suggesting widespread contamination of the samples.

For Table of Contents Only:

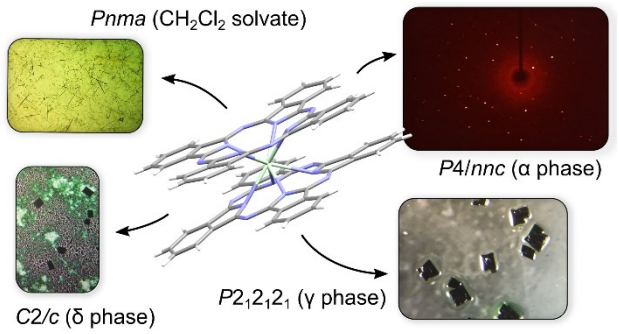

Four polymorphs of the phthalocyanine double deckers complexes are crystallized by solution evaporation methods, and their structures determined.